Optical Materials 148 (2024) 114789

Contents lists available at ScienceDirect

Optical Materials

journal homepage: www.elsevier.com/locate/optmat

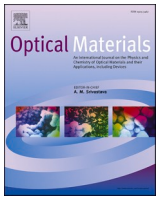

Research Article

Impact of a precise pH value change on the characteristics of deposited tin monosulphide films onto a flexible substrate

Noor M. Ibrahim [a], Manal M. Abdullah [a], Mohamed S. Mahdi [b,*]

[a] Department of Physics, College of Science, University of Baghdad, Iraq
[b] Environment, Water, and Renewable Energy Directorate, Ministry of Higher Education and Scientific Research, Iraq

ARTICLE INFO

Keywords:
Tin monosulphide
Chemical bath deposition
pH
Photodetector
Photoresponse

ABSTRACT

The chemical bath deposition technique (CBD) is considered the cheapest and easiest compared with other deposition techniques. However, it is highly sensitive to effective parameter deposition values such as pH, temperature, and so on. The pH value of the reaction solution has a direct impact on both the nucleation and growth rate of the film. Consequently, this study presents a novel investigation into the effect of a precise change in the pH reaction solution value on the structural, morphological, and photoresponse characteristics of tin monosulphide (SnS) films. The films were grown on a flexible polyester substrate with pH values of 7.1, 7.4, and 7.7. The X-ray diffraction patterns of the grown films at pH 7.1 and 7.4 confirmed their polycrystalline nature. Additionally, an observed alteration in the crystal structure occurred as the pH value increased from 7.1 to 7.4, resulting in a transition from an orthorhombic crystal structure to a cubic crystal structure. In contrast, the XRD pattern of the grown film at pH 7.7 revealed that it was amorphous. The field-emission scanning electron microscopy images revealed a flower-like morphology for the grown film at 7.1, whereas the grown films at 7.4 and 7.7 revealed a grain morphology. The results also showed that the pH values were also having an important effect on the energy gap value (E_g) of films; the E_g values were 1.46, 1.57, and 1.65 eV for pH 7.1, 7.4, and 7.7, respectively. The photodetectors fabricated using grown films exhibited excellent photoresponse characteristics when subjected to near-infrared (750 nm) illumination. It was also demonstrated that the photodetector using the cubic structure film possessed faster response times and greater sensitivity than the photodetector using the orthorhombic structure film.

1. Introduction

Nanostructured semiconductor materials have piqued the interest of researchers in recent years due to their distinctive characteristics in gas and light sensing [1]. Tin monosulphide has significant potential as a material due to its favorable characteristics, which include its environmentally sustainable nature, cost-efficiency, low cost, abundance on the earth, and absence of heavy metal components [2,3]. It also exhibits notable hole mobility, a substantial absorption coefficient exceeding 10^4 cm^{-1} [4,5], and a wide range of direct energy gap variations spanning from 1.1 to 1.6 eV [6]. The aforementioned attributes facilitate its utilization in a variety of applications, including gas sensors, photodetectors, solar cells, and so forth [7,8]. The SnS films primarily exhibit three crystal structures, namely zinc blende, orthorhombic, and cubic [9–11]. It is found that the type of crystal structure is strongly influenced by the deposition technique and its deposition parameters [12–14]. SnS films have previously been deposited using several kinds of methods, such as vacuum evaporation [15,16], sputtering [17], spray pyrolysis [18], chemical bath deposition (CBD) [11,14,19,20], and electrochemical deposition [21]. The CBD method is particularly important among these methods due to its simplicity and ease of obtaining large-area films [14,19,22–24]. Furthermore, it does not necessitate sophisticated equipment, and the deposition process can be performed at relatively low temperatures of less than 90 °C [25,26]. As a result, the flexible substrate can be used to deposit the films. The pH of the reaction solution directly affects the processes of nucleation and particle growth in films that are deposited on substrates [11,24,27,28]. Therefore, numerous studies have been undertaken to examine the impact of this effect on grown SnS films utilizing the CBD method [4,10,11,24,29]. However, the aforementioned studies did not specifically examine the precise alteration in pH levels. Instead, their focus was primarily on investigating the structural, morphological, and optical characteristics.

* Corresponding author.
E-mail address: msaleh196730@gmail.com (M.S. Mahdi).

https://doi.org/10.1016/j.optmat.2023.114789
Received 8 October 2023; Received in revised form 24 December 2023; Accepted 25 December 2023

Therefore, this study presents a novel investigation into how precisely changing the pH value affects the structural, morphological, and photoresponse characteristics of SnS films. The films were prepared onto a flexible (polyester) substrate. The findings indicated that there was a correlation between the pH value and the conversion of the crystal structure of films from orthorhombic to cubic. Additionally, there was significant variability observed in the photoresponse characteristics of the fabricated photodetectors based on the grown films.

2. Experimental part

2.1. Films preparation

SnS films were grown using the CBD technique. The S^{2-} and Sn^{2+} ions were obtained from 0.15 M thioacetamide (C_2H_5NS), and 0.1 M stannous chloride dehydrate ($SnCl_2.2H_2O$), respectively. As a complexing agent, 0.22 M dehydrate trisodium citrate ($C_6H_5Na_3O_7.2H_2O$) (TSC) was used, which helps to reduce the speed of precipitate during the deposition process of films. At room temperature, 50 mL of deionized water was used to dissolve the chemical materials while being stirred. Drop by drop, 25 % aqueous ammonium was added to the reaction solution to adjust the pH. Prior to the deposition of the film, ultrasonic cleaning with acetone, methanol, and deionized water was performed for 30 min on flexible polyester slide substrates. The duration of the deposition process was 2.5 h, conducted at a temperature of 80 °C. Subsequently, the substrates were extracted from the beaker, rinsed with deionized water, and left to air-dry. The SnS films were smooth and adhered well.

2.2. Film growth mechanism

Nucleation and growth are the two efficient mechanisms in the CBD method that govern the growth of films. The SnS film mainly occurs through three stages:

I-Ionization of stannous chloride in aqueous solution, according to following the reaction [30]:

$$SnCl_2 \rightarrow Sn^{2+} + 2Cl^- \quad (1)$$

II- The trisodium citrate dihydrate (TSC) [31] and Ammonia (NH_3) [32] were introduced as complexing agents for binding Sn^{+2} and resulting in Sn-complexing ions via the reactions described below:

$$Sn^{2+} + 2NH_3 \rightarrow Sn\ (NH_3)_2^{2+} \quad (2)$$

$$Sn^{2+} + TSC \rightarrow Sn\ (TSC)^{2+} \quad (3)$$

III-Finally, the Sn-complexing ions progressively dissolve to release Sn^{2+}. Then, these ions combine with the S^{2-} formed by the hydrolysis of thioacetamide to form the solid phase of SnS [33].

$$[SnLn]^{+2} + CSCH_3NH_2 + 2OH^- \rightarrow SnS + CH_3COONH_4 + nL \quad (4)$$

Where L referrers NH_3 or TSC. The nucleation as well as growth of the thin film are particularly affected by changes in pH (variation in the amount of NH_3 in the reaction solution). Increased pH causes more Sn^{2+} ions in the reaction solution to bond with NH_3 resulting in Sn-complexing ions (eq. (2)). Being that Sn-complexing ions dissolve slowly into free Sn^{2+} (eq. (4)), the growth rate slows. Concurrently, thioacetamide undergoes hydrolysis to produce S^{-2} ions, leading to the formation of chemical bonds with Sn^{2+} ions, ultimately resulting in the formation of the SnS phase. As the concentration of aqueous ammonia NH_3 in the solution increases, the concentration of free Sn^{2+} ions decreases, while the concentration of OH^{-1} ions increases. The increased concentration of OH^{-1} ions facilitates the hydrolysis of the S-precursor [34].

2.3. Films characterization

The structural characteristics of SnS films were analyzed using the X-ray diffraction (XRD) technique type Shimadzu (6000) Japanese diffractometer. The surface morphology of films was examined using field-emission scanning electron microscopy (FE-SEM), specifically the inspect f50 FE-SEM. The thickness of films was measured using atomic force microscopy (AFM) (Core 2023, Nano surf AG). The optical properties of films were investigated using absorption measurements within the wavelength range of (350–1100 nm) by UV–Vis spectrophotometer Shimadzu-2601. Lastly, the photoresponse measurements of fabricated photodetectors based on growing films were examined using a next-generation Keithley 2450 Source Meter unit (SMU), and a light-emitting diode (LED) illumination source at 750 nm.

3. Results and discussion

3.1. Crystal structure

Fig. 1 depicts the XRD patterns of films grown under varying pH conditions. The film deposited at pH 7.1 exhibits a diffraction peak at an angle of $2\theta = 31.59°$. This peak corresponds to the (111) plane of the SnS orthorhombic structure, according to JCPDS card 39–0354 [4,27,35,36]. At pH 7.4, the pattern of the deposited film shows two diffraction peaks at $2\theta = 31.88$ and $32.68°$, which correspond to the (410) and (411) planes of the SnS cubic structure [4,13,36,37], respectively. This reveals a significant change in crystal structure from orthorhombic to cubic because the pH increased from 7.1 to 7.4. In contrast, compared to the crystallinity nature of grown films at pH 7.1 and 7.4, the prepared film pattern at PH 7.7 exhibited an amorphous nature. According to the XRD results, the pH value has a significant impact on the type and nature of films crystallinity.

The Debye-Scherer equation was used to estimate crystallite size (D) along the (111) and (410), planes [38–42]:

$$D = 0.9\,\lambda/\beta\cos\theta \quad (5)$$

where λ denotes X-ray wavelength, θ is Bragg angle, and β denotes full width at half-maximum (FWHM).

The dislocation density (δ) value indicates the number of defects in the film. As a result, reducing the dislocation density in the film is necessary to fabricate high-quality thin films for use in optical devices, [40,43,44]. The micro-strain (ε), and dislocation density are determined for the (111) and (410) planes respectively using the following formulas [40,43,44]:

$$\epsilon = \frac{\beta}{4\tan} \quad (6)$$

$$\delta = \frac{1}{D^2} \quad (7)$$

The number of crystallites per unit area (N) are determined using the following equation [45]:

$$N = t/\,D^3 \quad (8)$$

where t is the thickness of grown films, which is determined by AFM measurements. This technique was employed in a previous study [46]. The thickness of the grown films measures 527, 371, and 220 nm at pH values of 7.1, 7.4, and 7.7, respectively. The XRD characteristics of the films grown at pH 7.1 and 7.4 are listed in Table 1. According to Table 1, the structural characteristics of grown film at pH 7.4 are better than those of grown film at pH 7.1. This can be attributed to a slow growth rate when the pH is increased (eq. (4)). The increasing the crystallite size can lead to fewer crystal defects, lower dislocation, and reduced boundaries. This, in turn, can improve the electrical properties of the film [40]. The D of grown film at pH 7.4 is greater than the reported

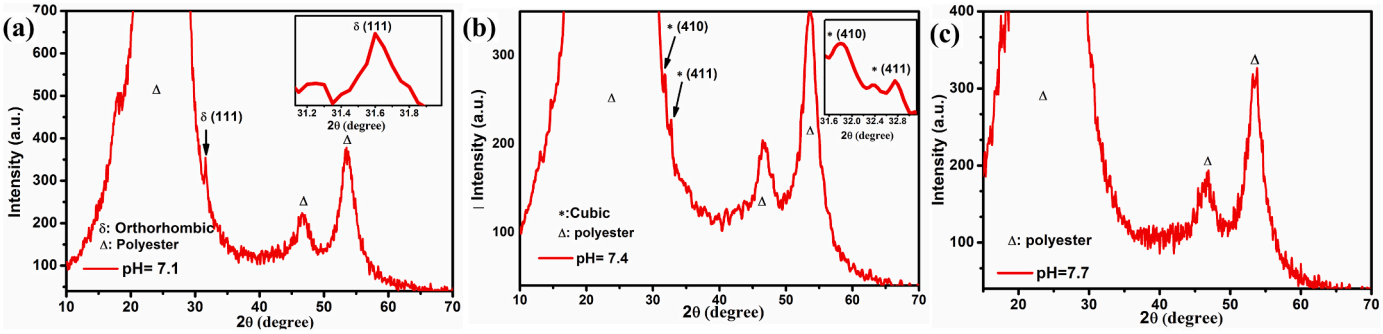

Fig. 1. XRD patterns of films growing at different pH values.

Table 1
The finding of structural characteristics of grown films at pH 7.1 and 7.4.

pH	t (nm)	(*hkl*)	D (nm)	$\epsilon \times 10^{-3}$	$\delta \times 10^{12}$ (lines cm^{-2})	$N \times 10^{14}$ (cm^{-2})
7.1	527	111	35.23	3.61	8.05	12.1
7.4	370	410	65.08	1.95	2.36	1.35
7.7	220	——	——	——	——	——

values in previous studies [31,40].

3.2. Surface morphology

Fig. 2 depicts the FE-SEM images of prepared SnS films obtained at different pH values. At pH 7.1, the surface of the SnS film (Fig. 2(a)) is covered with flower-shaped clusters that are close together. There are also several grains. The existence of a porous-like structure in the film surface will enhance light absorption, leading to an increase in the generation of electron-hole pairs. This, in turn, will result in an increase in the generated photocurrent and an enhancement in the performance of the photodetector [47]. The formation of the orthorhombic structure may be responsible for the presence of a flower-like morphology. This finding is consistent with previous research [10,34,48]. Furthermore, the presence of a cubic structure in the film may be attributed to the formation of grain morphology [4,10,13,49,50]. The assembled particle morphology completely covers the surface of the grown films at pH 7.4, and 7.7 (Fig. 2 (b, and c)). Furthermore, at pH 7.4, the surface of the film has a homogeneous distribution and a large particle size. In contrast, the surface of the grown film at pH 7.7 shows many small particles that have begun to agglomerate and form larger particles in the current study, the particle size distributions are displayed in the inset graphs, which are estimated using ImageJ software. The average particle sizes ($<D_{part}>$) were found to be 958, 189 and 122 nm for grown films at pH 7.1, 7.4, and 7.7, respectively.

3.3. Optical properties

The absorbance spectra of SnS films deposited on polyester substrates with different pH values are shown in Fig. 3(a). In general, the absorbance value increased with a decrease in wavelength for all films. Furthermore, the absorbance value of the film grown at pH 7.1 is greater than that of the films deposited at pH 7.4 and 7.7 in the 700–1100 nm range. This can be attributed to its thickness, which is the highest when compared to other thickness of films. Moreover, the surface morphology of film has a porous-like structure, which enhances light absorption [47].

The absorption coefficient in these films is calculated by using the following relation [51,52]:

$$\alpha = 2.303\frac{A}{t} \tag{9}$$

where α denotes the absorption coefficient, A is the absorbance.

To calculate the energy gap E_g and study the nature of optical transition behavior in films, the Tauc relation was employed [4,35,51,53,54]:

$$\alpha h\nu = B\left(h\nu - E_g\right)^n \tag{10}$$

where B is constant as a function of the transition, h is the Planck constant, ν is the frequency of the incident photon, E_g is energy gap, and n takes on varying values depending on the absorption process, and equal 1/2, 3/2, 2, and 3 for allowed, forbidden of direct and indirect transition respectively [30,55]. Fig. 3(b–d) shows a plot of the $(\alpha h\upsilon)^2$ as a function of incident energy ($h\upsilon$), assuming n = 2. The finding suggests that the films have a direct optical transition instead of depending on phonons.

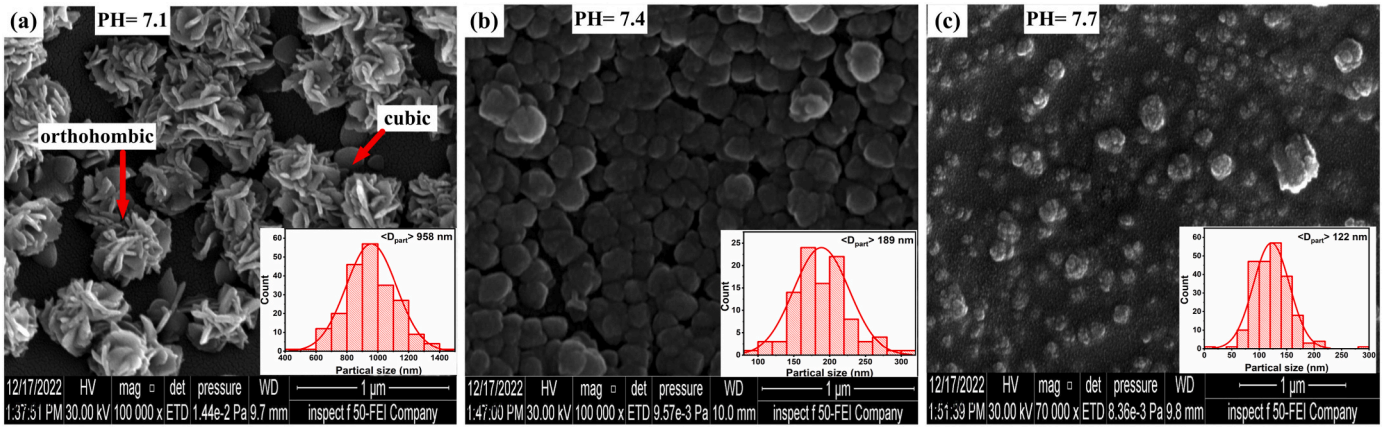

Fig. 2. FE-SEM images of SnS films at various pH values.

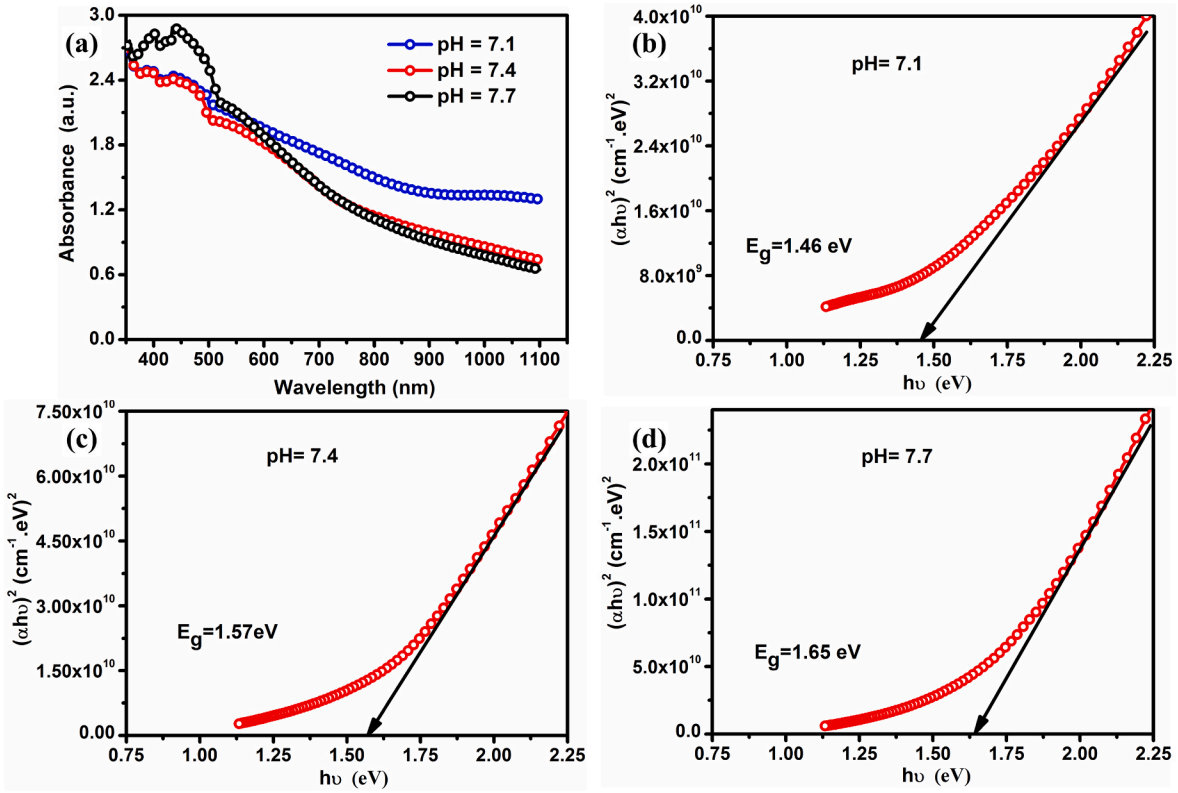

Fig. 3. Plots of a) absorbance vs. wavelength, and (b–d) (αhν) ^2 vs. (hν) for prepared films.

The direct energy gap was determined by extrapolating the straight line of $(\alpha h\upsilon)^2$ versus the hυ curve to intercept the horizontal hυ axis. E_g values for grown films at pH 7.1, 7.4, and 7.7 were estimated to be 1.46, 1.57, and 1.65 eV, respectively. The findings revealed that films with an orthorhombic crystal structure have a lower energy band gap than films with cubic structure, which is consistent with prior studies [4,35,51,53,54]:

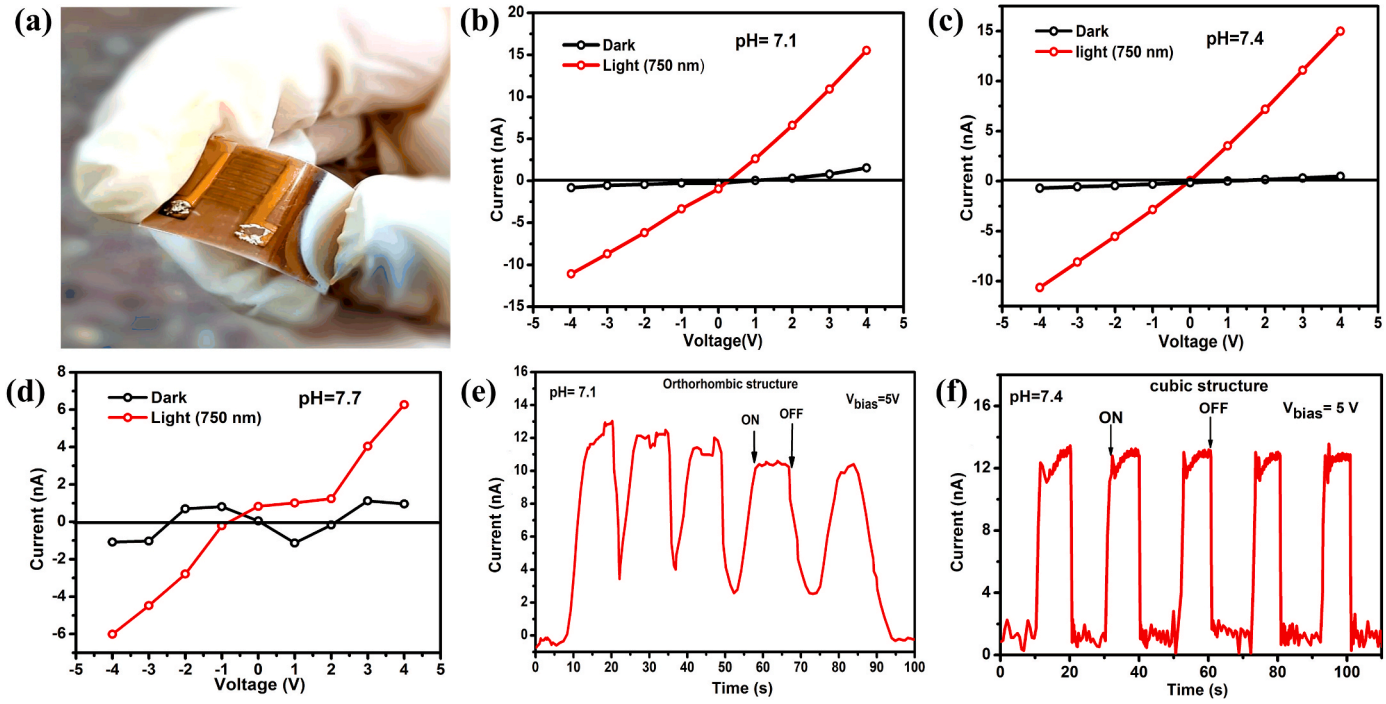

Fig. 4. (a) Real image of fabricated photodetector onto flexible polyester substrate, (b–d) the I–V characteristics of the photodetectors in the dark and under illumination, (e, and f) I-T characteristics of the photodetectors measured at 5 V bias voltage.

3.4. Photoresponse characteristics

The ion coating method was used four times to deposit gold (Au) electrodes with a thickness of 120 nm to construct metal-semiconductor-metal (M-S-M) photodetectors. The electrodes were deposited through a finger mask. A real image of photodetector is shown in Fig. 4(a). Fig. 4 (b–d) depicts the current-voltage (I–V) curves of the devices in the dark and under light illumination in near-infrared (750 nm) conditions. It is notable that the current value increases significantly upon illumination when compared to the dark state for photodetectors based on depositing films at pH 7.1 and 7.4. In contrast, it is not for the photodetector based on film deposition at pH 7.7; the current value displayed zigzag behavior. The zigzag shape appears in the dark due to a low dark current value of approximately 1 nA at 4 voltage and less at lower voltages. As a result, any fluctuations in its value are observable. However, the light current value is approximately 6 nA at 4 V. As a consequence, little fluctuations in light current value was noticed. This result may be attributed to the amorphous nature of the growing film at pH 7.7 (Fig. 1 (c)).

Repeatability and photoresponse speed are crucial characteristics in determining the capability of a photodetector application. The photoresponse of device stability was examined at a 5 V bias voltage with a 10 s ON/OFF switch cycle, as illustrated in Fig. 4 (e and f). It is noticeable that after a number of cycles, the maximum value of the current remains constant and unchanged for the photodetector based on grown film at pH 7.4 (Fig. 4 (f)), confirming the outstanding reproducibility and stability of the device. However, these features are not available in photodetectors based on grown film at pH 7.1 (Fig. 4 (e)). Furthermore, despite the presence of a porous structure in the grown film at pH 7.1, the results show that the photocurrent of photodetector is approximately 9 nA. This value is less than the photocurrent of photodetector at pH 7.4, which is approximately 13 nA. This can be attributed to the mean free path of electrons in motion, which is inversely proportional to both the number of crystallites per unit area and the film thickness (as shown in Table 1).

The sensitivity of a photodetector is defined as the ratio of an increase in current when illuminated to a dark current [54]. The sensitivity (S) can be stated as follows [30,54,56–60]

$$S = \frac{I_{ph}}{I_{dark}}\, x100 \tag{11}$$

where $I_{ph} = I_{light} - I_{dark}$. I_{dark} and I_{light} are the dark, and under illumination currents, respectively. The S values were found to be 801 and 1775 for the fabricated photodetectors based on grown film at pH 7.1 and 7.4, respectively. The S value of fabricated photodetector using grown film at pH 7.4 is highest compared to previously reported values for fabricated photodetectors based on grown films on glass and PET substrates [4,11, 12,15,25,30,34,54,58–60], which were tabulated in Table 2. The photoresponse time is critical for studying the performance of the photodetector, and a significantly faster response time has the potential to broaden the field of photodetector applications. The rise times of a single on/off cycle were approximately 1.6 s and 0.72 s, while the decay times were 1.9 s and 0.68 s for devices manufactured using SnS films deposited at pH 7.1 and 7.4, respectively.

The photosensitivity and photoresponse time results demonstrated that the fabricated photodetector based on cubic crystal structure shows excellent photoresponse characteristics compared to that based on orthorhombic crystal structure. This difference can be attributed to crystal structure characteristics, where increased grain boundary scattering through film could lead to detrimental carrier scattering at small crystallite sizes, which results in a significant decrease in charge carrier mobility [61], as well as the good crystal quality reduces the density of traps induced by defects. Moreover, the decrease of carrier's mobility with impurity concentration due to carriers scattering [62,63]. Thus, the photocurrent reaches a steady state rapidly during both rise and decay stages [64].

The findings of the photoresponse measurements (I–V and I-T curves) showed that the pH value has a direct influence on the crystalline structure of the grown films, which influences the sensitivity and photoresponse time values of photodetectors.

4. Conclusions

The present study highlighted the influence of a precise change in pH value (7.1.7.4 and 7.7) on the properties of grown SnS films on flexible polyester substrates. The obtained findings revealed that the pH value has a significant impact on the type of crystal structure (orthorhombic and cubic), morphology and photoresponse properties of deposited films. The performance of fabricated photodetectors based on deposited films has a significant correlation with their type of crystal structure; the sensitivity was determined to be 801 and 1775 for photodetectors based on growing films that crystallized in orthorhombic and cubic structures, respectively. The findings of this study pave the way for the potential use of SnS films with cubic crystal structures as basic components in the fabrication of flexible near-infrared photodetectors in future research objectives.

CRediT authorship contribution statement

Noor M. Ibrahim: Data curation, Formal analysis, Methodology, Resources, Writing – original draft, Writing – review & editing. **Manal M. Abdullah:** Formal analysis, Methodology, Supervision, Validation, Visualization, Writing – original draft. **Mohamed S. Mahdi:** Conceptualization, Data curation, Formal analysis, Investigation, Methodology, Resources, Supervision, Validation, Visualization, Writing – original draft, Writing – review & editing.

Table 2
A comparison of photoresponse findings for present SnS photodetectors with previously published research for fabricated photodetectors based on grown SnS films on glass and PET substrates.

Substrate	Crystal structure	Bias Voltage (V)	Illumination Source	Power density mW/cm^2	Rise/decay Times (s)	Sensitivity %	References
Glass	Orthorhombic	10	Tungsten halogen lamp	100	——	~250	[11]
Glass	Orthorhombic	5	Visible light	100	——	80	[15]
Glass	Orthorhombic	4	Tungsten halogen lamp	100	——	~157	[30]
Glass	Orthorhombic	5	750 nm	38	2.81/4.27	260	[54]
Glass	Orthorhombic	5	750 nm	38	——	170	[58]
Glass	Orthorhombic	5	532 nm	5	5.3/5.1	~50	[59]
Glass	Orthorhombic	5	532 nm	——	1.5/2.5	~96	[60]
PET	Orthorhombic	5	750 nm	38	0.19/0.28	404	[25]
PET	Orthorhombic	5	850 nm	55	0.20/0.26	312	[34]
Polyester	Orthorhombic	5	750 nm	27	1.6/1.9	801	This work
Glass	Cubic	5	750 nm	38	0.44/0.5	700	[4]
PET	Cubic	5	750 nm	38	0.55/0.53	1635	[12]
Polyester	Cubic	5	750 nm	27	0.72/0.68	1775	This work

Declaration of competing interest

On behalf of my co-authors, I certify that all authors have seen and approved the final version of the submitted manuscript. The manuscript is original and has not been published elsewhere, and is not currently under submission to any other journal, and will not be submitted elsewhere before a decision is made by this journal.

Data availability

No data was used for the research described in the article.

Acknowledgments

The authors express their gratitude to the environment, water, and renewable energy directorate, Ministry of Science and Technology-Iraq for providing support to this research project.

References

[1] F. Lu, J. Yang, R. Li, N. Huo, Y. Li, Z. Wei, J. Li, J. Mater. Chem. 3 (2015) 1397–1402.
[2] E.C. Greyson, J.E. Barton, T.W. Odom, Small 2 (2006) 368–371.
[3] J. H, T.Z. Xing Zhou, Lin Gan, Qi Zhang, Xiong Xing, Huiqiao Li, Zhiqiang Zhong, J. Mater. Chem. 4 (2016) 2111.
[4] M.S. Mahdi, K. Ibrahim, N.M. Ahmed, A. Hmood, S.A. Azzez, F.I. Mustafa, M. Bououdina, Mater. Lett. 210 (2018) 279–282.
[5] M. Devika, K.T. Ramakrishna Reddy, N. Koteeswara Reddy, K. Ramesh, R. Ganesan, E.S.R. Gopal, K.R. Gunasekharr, J. Appl. Phys. 100 (2006).
[6] Julien Vidal, Stephan Lany, Mayeul d'Avezac, Alex Zunger, Andriy Zakutayev, Jason Francis, Janet Tate, Appl. Phys. Lett. 100 (2012), 032104.
[7] R.E. Abutbul, E. Segev, L. Zeiri, V. Ezersky, G. Makov, Y. Golan, RSC Adv. 6 (2016) 5848–5855.
[8] K. Ramasamy, V.L. Kuznetsov, K. Gopal, M.A. Malik, J. Raftery, P.P. Edwards, P. O'Brien, Chem. Mater. 25 (2013) 266–276.
[9] J. Breternitz, R. Gunder, H. Hempel, S. Binet, I. Ahmet, S. Schorr, Inorg. Chem. 56 (2017) 11455–11457.
[10] I.G. Marquez, R. Romano-Trujillo, J.M. Gracia-Jimenez, R. Galeazzi, N.R. Silva-Gonzalez, G. Garcıa, A. Coyopol, F.G. Nieto-Caballero, E. Rosendo, C. Morales, J. Mater. Sci. Mater. Electron. 32 (2021) 15898–15906.
[11] C. Gao, H. Shen, L. Sun, Appl. Surf. Sci. 257 (2011) 6750–6755.
[12] M.S. Mahdi, N.M. Ahmed, A. Hmood, K. Ibrahim, M. Bououdina, Mater. Sci. Semicond. Process. 100 (2019) 270–274.
[13] A.R. Garcia-Angelmo, R. Romano-Trujillo, J. Campos Alvarez, O. Gomez-Daza, M. T.S. Nair, P.K. Nair, Phys. Status Solidi 212 (2015) 2332–2340.
[14] E. Guneri, F. Gode, C. Ulutas, F. Kirmizigul, G. Altindemir, C. Gumus, Chalcogenide Lett. 7 12 (2010) 685–694.
[15] T. Srinivasa Reddy, M.C. Santhosh Kumar, RSC Adv. 6 (2016) 95680–95692.
[16] R.W. Miles, O.E. Ogah, G. Zoppi, I. Forbes, Thin Solid Films 517 (2009) 4702–4705.
[17] K. Hartman, J.L. Johnson, M.I. Bertoni, D. Recht, M.J. Aziz, M.A. Scarpulla, T. Buonassisi, Thin Solid Films 519 (2011) 7421–7424.
[18] M. Calixto-Rodriguez, H. Martinez, A. Sanchez-Juarez, J. Campos-Alvarez, A. Tiburcio-Silver, M.E. Calixto, Thin Solid Films 517 (2009) 2497–2499.
[19] A. Tanuševski, D. Poelman, Sol. Energy Mater. Sol. Cells 80 (2003) 297–303.
[20] E. Turan, M. Kul, A.S. Aybek, M. Zor, J. Phys. D Appl. Phys. 42 (2009), 245408.
[21] S. Cheng, Y. Chen, Y. He, G. Chen, Mater. Lett. 61 (2007) 1408–1412.
[22] U. Chalapathi, B. Poornaprakash, S. Park, Superlattice. Microst. 103 (2017) 221–229.
[23] Y. Jayasree, U. Chalapathi, V.S. Raja, Thin Solid Films 537 (2013) 149–155.
[24] C. Gao, H. Shen, L. Sun, Z. Shen, Mater. Lett. 65 (2011) 1413–1415.
[25] Mohamed S. Mahdi, Husam S. Al-Arab, Kamal H. Latif, K. Ibrahim, M. Bououdina, Appl. Phys. A 126 (2020) 958.
[26] Inderjeet Kaur, D.K. Pandya, K.L. Chopra, J. Electrochem. Soc. 127 (1980) 943.
[27] M. Ristov, G.J. Sinadinovski, I. Grozdanov, M. Mitreski, Thin Solid Films 173 (1989) 53–58.
[28] T.H. Sajeesh, A.S. Cherian, C.S. Kartha, Energy Proc. 15 (2012) 325–332.
[29] A. Higareda-Sanchez, R. Mis-Fernandez, I. Rimmaudo, E. Camacho-Espinosa, J. L. Pena, Superlattice. Microst. 151 (2021), 106831.
[30] M. Cao, C. Wu, K. Yao, J. Jing, J. Huang, M. Cao, J. Zhang, J. Lai, O. Ali, L. Wang, Y. Shen, Mater. Res. Bull. 104 (2018) 244–249.
[31] M.S. Mahdi, H.S. Al-Arab, H.S. Al-Salman, K. Ibrahim, N.M. Ahmed, A. Hmood, M. Bououdina, Mater. Lett. 273 (2020) 5–8.
[32] A. Antony, K.V. Murali, R. Manoj, M.K. Jayaraj, Mater. Chem. Phys. 90 (2005) 106–110.
[33] M.T.S. Nair, P.K. Nai, Semicond. Sci. Technol. 6 (1991) 132.
[34] M.S. Mahdi, K.H. Latif, A.A. Jabor, K. Ibrahim, N.M. Ahmed, A. Hmood, F. I. Mustafa, M. Bououdina, J. Electron. Mater. 49 (2020) 5824–5830.
[35] A. Javed, Nauman Khan, S. Bashir, M. Ahmad, Mater. Chem. Phys. 246 (2020), 122831.
[36] P.K. Nair, A.R. Garcia-Angelmo, M.T.S. Nair, Phys. Status Solidi 213 (2016) 170–177.
[37] V.E. González-Flores, R.N. Mohan, R. Ballinas-Morales, M.T.S. Nair, P.K. Nair, Thin Solid Films 672 (2019) 62–65.
[38] A.M. Suhail, M.J. Khalifa, N.M. Saeed, O.A. Ibrahim, EPJ Appl. Phys. 49 (2010) 1–5.
[39] M.K. Khalaf, S.N. Mazhir, M.S. Mahdi, S.K. Taha, M. Bououdina, Mater. Res. Express 6 (2019) 1–10.
[40] L.A. Rodríguez-Guadarrama, J. Escorcia-García, I.L. Alonso-Lemus, J. Campos-Álvarez, J. Mater. Sci. Mater. Electron. 32 (2021) 7464–7480.
[41] R.A. Ghazi, A.J. Ghazai, Z.M. Shaban, K.H. Abass, N.F. Habubi, S.S. Chiad, J. Nanostructures 11 (2021) 66–72.
[42] M.M. Abdullah, M.H. Suhail, S.I. Abbas, Arch. Appl. Sci. Res. 4 (2012) 1279–1288.
[43] M.S. Mahdi, K. Ibrahim, A. Hmood, N.M. Ahmed, F.I. Mustafa, J. Electron. Mater. 46 (2017) 4227–4235.
[44] M.I. Khan, S. Hussain, M. Fatima, S. Bano, M.S. Hasan, I. Bashir, M. Ammami, Inorg. Chem. Commun. 157 (2023), 111361.
[45] M.M. El-Nahass, Z. El-Gohary, H.S. Soliman, Opt Laser. Technol. 35 (2003) 523–531.
[46] F. Gode, E. Guneri, O. Baglayan, Appl. Surf. Sci. 318 (2014) 227–233.
[47] Lou Zheng, Ludong Li, Guozhen Shen, Nanoscale 8 (2016) 5219–5225.
[48] C. Guneri, E. Ulutas, C. Kirmizigul, F. Altindemir, G. Gode, F. Gumus, Appl. Surf. Sci. 257 (2010) 1189–1195.
[49] A.R. Garcia-Angelmo, M.T.S. Nair, P.K. Nair, Solid State Sci. 30 (2014) 26–35.
[50] Mohamed S. Mahdi, S. Husam, Al-Arab, A. Hmood, M. Bououdina, Opt. Mater. 123 (2022), 111910.
[51] S. Suresh, J. Cryst. Process Technol. 3 (2013) 87–91.
[52] Y. Doubi, B. Hartiti, H. Labrim, S. Fadili, M. Tahri, A. Belafhaili, M. Siadat, P. Thevenin, Appl. Phys. Mater. Sci. Process 127 (2021) 1–11.
[53] Y. Tao, X. Wu, W. Wang, J. Wang, J. Mater. Chem. C 3 (2015) 1347–1353.
[54] M.S. Mahdi, A. Hmood, K. Ibrahim, N.M. Ahmed, M. Bououdina, Superlattice. Microst. 128 (2019) 170–176.
[55] Maab A. Abood, Bushra A. Hasan, Iraqi J. Sci. 64 (2023) 1675–1690.
[56] P. Kumar, N. Saxena, S. Dewan, F. Singh, V. Gupta, RSC Adv. 6 (2016) 3642–3649.
[57] K.M. Chahrour, N.M. Ahmed, M.R. Hashim, N.G. Elfadill, M. Bououdina, Sensors Actuators A Phys 239 (2016) 209–219.
[58] M.S. Mahdi, K. Ibrahim, N.M. Ahmed, A. Hmood, S.A. Azzez, Solid State Phenom. 290 (2019) 220–224.
[59] R.G. Devarajan Alagarasana, S.S. Hegde, S. Varadharaja perumal, R. Aadhavan, R. Naikd, Mohd Shkire, H. Algarnie, Phys. Scripta 97 (2022) 1–19.
[60] R. Balakarthikeyan, A. Santhanam, Aslam Khan, Ahmed M. El-Toni, Anees A. Ansari, Ahamad Imran, Mohd Shkir, S. AlFaify, Optik 244 (2021), 167460.
[61] Nikhil Satyala, Daryoosh Vashaee, Appl. Phys. Lett. 100 (2012), 073107.
[62] Zhigang Zang, Atsushi Nakamura, Jiro Temmyo, Opt Express 21 (2013) 11448–11456.
[63] C. Hilsum, Electron. Lett. 10 (1974) 259–260.
[64] J.S. Jie, W.J. Zhang, Y. Jiang, X.M. Meng, Y.Q. Li, S.T. Lee, Nano Lett. 6 (2006) 1887–1892.